

# COMPUTATION OF SYNTHETIC SPECTRA FROM SIMULATIONS OF RELATIVISTIC SHOCKS

BRIAN REVILLE AND JOHN G. KIRK

Max-Planck-Institut für Kernphysik, Postfach 10 39 80, 69029 Heidelberg, Germany

*Draft version March 13, 2022*

## ABSTRACT

Particle-in-cell (PIC) simulations of relativistic shocks are in principle capable of predicting the spectra of photons that are radiated incoherently by the accelerated particles. The most direct method evaluates the spectrum using the fields given by the Liénard-Wiechart potentials. However, for relativistic particles this procedure is computationally expensive. Here we present an alternative method, that uses the concept of the photon formation length. The algorithm is suitable for evaluating spectra both from particles moving in a specific realization of a turbulent electromagnetic field, or from trajectories given as a finite, discrete time series by a PIC simulation. The main advantage of the method is that it identifies the intrinsic spectral features, and filters out those that are artifacts of the limited time resolution and finite duration of input trajectories.

*Subject headings:* radiation mechanisms: general — methods: numerical — gamma-ray burst: general — relativistic processes

## 1. INTRODUCTION

Particle acceleration at relativistic shocks is thought to be responsible for the high-energy nonthermal photons observed from a variety of astrophysical objects, such as gamma-ray bursts, pulsars and blazars. To test this hypothesis, reliable predictions of the photon spectra are needed. Analytic models have been used to provide estimates of the expected asymptotic power-law index at high energy and the maximum attainable photon energy (Derishev 2007; Kirk & Reville 2010), but they cannot currently take account of potentially important effects, such as the role of self-generated turbulence in the vicinity of the shock. Particle in cell (PIC) simulations, on the other hand, have the potential to capture these effects, and have recently begun to provide evidence that Fermi acceleration is a natural consequence of relativistic shock formation (Spitkovsky 2005, 2008a,b; Sironi & Spitkovsky 2009a; Martins et al. 2009b). In principle, these simulations are capable of reproducing the essential physics; they are *ab initio* in the sense that all processes are reproduced by evolving the electromagnetic fields and the particle distribution according to the classical equations of motion and Maxwell's equations.

However, to compare the simulations with observations, it is essential to understand the predicted radiative signatures. Using results from PIC simulations, several groups have computed the emission at relativistic shocks (Hededal 2005; Martins et al. 2009a; Sironi & Spitkovsky 2009b; Medvedev et al. 2010), but the results show substantial differences. This is not necessarily due to the way in which the spectra were evaluated, since the electromagnetic fields and energetic particle distribution vary strongly from simulation to simulation. On the other hand, it does not rule out such a dependence. In each case, the method employed to compute the emission is the same: the electric field produced at a virtual detector by a single particle trajectory is evaluated using the Liénard-Wiechart potentials, the result is Fourier transformed and then averaged over a

large family of trajectories. This procedure is expensive in terms of computing resources, especially if one wants to compute the high-energy emission of relativistic particles, because of (i) the extremely high time resolution required to describe high-energy photons, (ii) the large number of virtual detectors required to resolve the narrow radiation beam of a relativistic particle (which scales as  $\gamma^2$ ) and (iii) the long time series needed to account for low-frequency emission.

In this paper, we present an alternative approach. For a given observing frequency, we identify at each point on a particle trajectory the length that contributes coherently to the emission. In a quantum picture, this is known as the photon formation length (Akhiezer & Shul'ga 1987). Using this as a guide, we then perform the integrations using a new algorithm that is optimized for highly relativistic particles.

The essential information on the particle trajectory can be supplied to the algorithm in two different ways: If the electromagnetic fields are prescribed as a function of space and time, then the trajectory can be integrated using standard adjustable-step methods. As examples, we present in section 3 computations of the emission spectrum from isotropic particle distributions immersed in stationary, turbulent magnetic fields. In this case, the algorithm is employed in the inner loop of a multi-dimensional integration, which is performed using a Monte-Carlo method. On the other hand, if the fields are not known at all points in space and time, interpolation is required. This is the case, for example, in PIC simulations, where the fields, particle positions and velocities are known only at discrete times and locations. We discuss this situation and suggest a procedure for implementing the algorithm in section 4.

## 2. EQUATIONS FOR THE EMISSIVITY

In the classical theory of electrodynamics, the spectral and angular distribution of radiation produced by a single particle in vacuum in the direction  $\mathbf{n}$  is given by the

well-known formula (e.g. Landau & Lifshitz 1971)

$$\frac{dE}{d\omega d\Omega} = \frac{q^2}{4\pi^2 c} \left| \int_{-\infty}^{+\infty} \frac{\mathbf{n} \times [(\mathbf{n} - \boldsymbol{\beta}) \times \dot{\boldsymbol{\beta}}]}{(1 - \mathbf{n} \cdot \boldsymbol{\beta})^2} e^{i(\omega t - \mathbf{k} \cdot \mathbf{x}(t))} dt \right|^2 \quad (1)$$

where  $\mathbf{k} = \omega \mathbf{n}/c$ . Equation (1) is usually used as the starting point for the numerical computation of radiation signatures from PIC codes — a detailed description of the method can be found in Hededal (2005). However, there are three disadvantages of this form of the emissivity

1. the term  $e^{i\omega t}$  is rapidly oscillating
2. the term  $1 - \mathbf{n} \cdot \boldsymbol{\beta}(t)$  in the denominator produces a very sharply peaked function when used for the trajectory of a relativistic particle
3. the range of integration extends over the entire section of the trajectory on which the acceleration is nonzero, making it difficult to relate the expression to a local emissivity and, hence, to compute time-dependent emission.

Straightforward transformations lead to a number of alternative forms for Equation (1), for example,

$$\frac{dE}{d\omega d\Omega} = \int_{-\infty}^{\infty} P(\mathbf{n}, \omega, t) dt \quad (2)$$

where

$$P(\mathbf{n}, \omega, t) = -\frac{q^2 \omega^2}{4\pi^2 c} \int_{-\infty}^{\infty} d\tau [1 - \boldsymbol{\beta}(t + \tau) \cdot \boldsymbol{\beta}(t)] \cos(\omega [\tau - \mathbf{n} \cdot (\mathbf{x}(t + \tau) - \mathbf{x}(t))/c]) \quad (3)$$

This expression is exact, and has the advantage that, provided variations on the timescale  $\omega^{-1}$  are small, the quantity  $P(\mathbf{n}, \omega, t)$ , when suitably averaged, can be interpreted as the instantaneous spectral power radiated per unit solid angle about the direction  $\mathbf{n}$  (Schwinger 1949).

In practice, it is necessary to truncate the integrals in (2) and (3) to finite intervals. From the form of the integrand in (3), it is clear that the endpoints should be chosen such that at least the first few periods of the cosine function are included. This leads to the concept of the photon formation time or coherence time, which applies to both the quantum and classical formulations of the problem (for a review, see Akhiezer & Shul'ga 1987). For a given Fourier mode, with wavelength  $\lambda = 2\pi c/\omega$ , a particle trajectory contributes coherently to the instantaneous power radiated at time  $t$  until it has lagged at least one wavelength behind the wavefront emitted at time  $t$ . Thus, the coherence or formation time  $\tau_{\text{coh}}$  is determined implicitly by the equation

$$\omega (\tau_{\text{coh}} - |\mathbf{x}(t + \tau_{\text{coh}}) - \mathbf{x}(t)|/c) = 2\pi \quad (4)$$

To compute the radiated power, one needs to know the trajectory accurately over several coherence times. For relativistic particles, a wavefront can take a considerable amount of time to separate one wavelength from the particle, particularly at low frequencies, when the wavelength is long.

In the context of Fermi acceleration at relativistic shocks, an angular dependent calculation of the emission from an individual particle is unnecessary, provided one is interested only in the high-energy emission from accelerated particles. This is because the characteristic radiation beaming angle of  $1/\gamma$  is much smaller for these particles than the scales on which anisotropy in the particle distribution can be expected, which is roughly the reciprocal of the Lorentz factor of the fluid motion into the shock (Achterberg et al. 2001). Hence, when summed over all plasma particles, these sharp emission peaks are smoothed out. In this case, it is advantageous to work with an angle-integrated expression for the individual particle spectrum. Integrating equation (3) over solid angle, gives:

$$\frac{dE}{d\omega} = \int_{-\infty}^{\infty} P(\omega, t) dt \quad (5)$$

where

$$P(\omega, t) = \frac{e^2 \omega}{2\pi c} \int_{-\infty}^{\infty} d\tau [1 - \boldsymbol{\beta}(t) \cdot \boldsymbol{\beta}(t + \tau)] F(\omega, t, \tau) \quad (6)$$

with

$$F(\omega, t, \tau) = \frac{\sin[\omega(\tau - \Delta)] - \sin[\omega(\tau + \Delta)]}{\Delta} \quad (7)$$

$$\Delta(t, \tau) = |\mathbf{x}(t + \tau) - \mathbf{x}(t)|/c \quad (8)$$

Equation (6) is also exact, and  $P(\omega, t)$  can be interpreted as the power radiated at time  $t$  in unit angular frequency range, again subject to the condition that it varies slowly on the timescale  $\omega^{-1}$  (Schwinger 1949). This condition is not always fulfilled for the trajectories we consider. In particular, it is violated when the acceleration felt by the particle fluctuates rapidly whilst the velocity remains within the beaming angle of the radiation (“jitter” radiation). Nevertheless, equation (5) for the total radiated energy remains valid, although  $P(\omega, t)$ , which we call the “instantaneous power”, is not necessarily positive definite.

### 2.1. Computation of the instantaneous power

For relativistic particles, and for small  $\tau$ , such that the particle displacement  $\Delta$  defined in (8) is approximately  $\beta|\tau|$ , the function  $F(\omega, t, \tau)$  in (7) contains two kinds of term: those that oscillate rapidly in  $\tau$  with frequency  $\sim \omega$ , and those that oscillate slowly, with frequency  $\omega/\gamma^2$ . Physically, the latter arise because the particle chases the wavefront, remaining close to it for a relatively long time. It is convenient to separate these terms:

$$P(\omega, t) = P_1(\omega, t) + P_2(\omega, t) \quad (9)$$

$$P_1(\omega, t) = \frac{e^2 \omega}{2\pi c} \int_{-\infty}^{\infty} d\tau [1 - \boldsymbol{\beta}(t) \cdot \boldsymbol{\beta}(t + \tau)] \frac{\sin\left[\omega\tau\left(1 - \frac{\Delta}{|\tau|}\right)\right]}{\tau\Delta/|\tau|} \quad (10)$$

$$P_2(\omega, t) = -\frac{e^2 \omega}{2\pi c} \int_{-\infty}^{\infty} d\tau [1 - \boldsymbol{\beta}(t) \cdot \boldsymbol{\beta}(t + \tau)] \frac{\sin\left[\omega\tau\left(1 + \frac{\Delta}{|\tau|}\right)\right]}{\tau\Delta/|\tau|} \quad (11)$$

In the case of  $P_2$ , the time  $\tau$  over which the trajectory is sampled is very short,  $\sim 1/\omega$ , whereas in the case of  $P_1$  it is much longer,  $\sim \gamma^2/\omega$ . To develop an approximation scheme for these terms we introduce quantities that describe the deviation of the trajectory from ballistic motion. These are the deviation in position

$$\delta\mathbf{x}(t, \tau) = \mathbf{x}(t + \tau) - \mathbf{x}(t) - c\tau\boldsymbol{\beta}(t), \quad (12)$$

the deviation in velocity:

$$\delta\boldsymbol{\beta}(t, \tau) = \boldsymbol{\beta}(t + \tau) - \boldsymbol{\beta}(t) \quad (13)$$

and the deviation of the displacement

$$\delta\Delta(t, \tau) = \Delta(t, \tau) - |\tau|\beta(t). \quad (14)$$

Clearly, to zeroth order in these deviations, the instantaneous power must vanish, since a particle undergoing uniform motion does not radiate. Furthermore, because of the relatively long sampling time, the dominant higher order contributions in the deviations come from  $P_1$ . For frequencies large compared to the instantaneous angular frequency (the local gyrofrequency), the higher order contributions in the  $P_2$  term can be neglected to give

$$P(\omega, t) \approx \frac{e^2\omega}{2\pi c} \int_{-\infty}^{\infty} d\tau \left\{ [1 - \beta^2(t) - \boldsymbol{\beta}(t) \cdot \delta\boldsymbol{\beta}(t, \tau)] \frac{\sin g(\omega, t, \tau)}{\tau [\beta(t) + \delta\Delta(t, \tau)/|\tau|]} - [1 - \beta^2(t)] \frac{\sin [\omega\tau(1 + \beta(t))]}{\tau\beta(t)} \right\} \quad (15)$$

where we have introduced the phase-lag  $g(\omega, t, \tau)$ :

$$g(\omega, t, \tau) = \omega\tau \left[ 1 - \beta(t) - \frac{\delta\Delta(t, \tau)}{|\tau|} \right] \quad (16)$$

At this point it would be possible to proceed by evaluating analytically the integral involving the second term in (15):

$$\frac{1}{\gamma^2(t)\beta(t)} \int_{-\infty}^{\infty} d\tau \frac{\sin [\omega\tau(1 + \beta(t))]}{\tau} = \frac{\pi}{\gamma^2(t)\beta(t)} \quad (17)$$

Indeed, Schwinger (1949) followed this path in deriving an analytic expression for the synchrotron emissivity. However, because the integrands are oscillatory, it is instead preferable to group them together. Transforming the integration variable from  $\tau$  to the phase-lag  $g$  defined in (16), in the case of the first term in (15), and as  $g = \omega\tau(1 + \beta(t))$  in the case of the second term, leads to

$$P(\omega, t) = \frac{e^2\omega}{2\pi c} \int_{-\infty}^{\infty} dg \frac{\sin g}{g} \left\{ \left[ \frac{1}{\gamma^2(t)\beta(t)} \right] \left[ \frac{\beta(t)g}{\tau\dot{g} \left[ \beta(t) + \frac{\delta\Delta(t, \tau)}{|\tau|} \right]} - 1 \right] - \frac{g\boldsymbol{\beta}(t) \cdot \delta\boldsymbol{\beta}(t, \tau)}{\dot{g}\tau \left[ \beta(t) + \frac{\delta\Delta(t, \tau)}{|\tau|} \right]} \right\} \quad (18)$$

where

$$\begin{aligned} \dot{g} &= \frac{\partial g}{\partial \tau} \\ &= \omega - \frac{\omega\boldsymbol{\beta}(t + \tau) \cdot [\mathbf{x}(t + \tau) - \mathbf{x}(t)]}{c\tau\Delta(t, \tau)/|\tau|} \\ &= \omega - \frac{\omega \{ [\boldsymbol{\beta}(t) + \delta\boldsymbol{\beta}(t, \tau)] \cdot [c\tau\boldsymbol{\beta}(t) + \delta\mathbf{x}(t, \tau)] \}}{c\tau \left[ \beta(t) + \frac{\delta\Delta(t, \tau)}{|\tau|} \right]} \end{aligned} \quad (19) \quad (20)$$

As required,  $P$  vanishes to zeroth order in the deviations from a ballistic orbit, (12), (13) and (14). The grouping of the terms in Equation (18) in this manner is especially important at high frequencies, where the higher order terms in  $P_1$  and  $P_2$  are small. In this limit, the two terms can be expressed as

$$\lim_{\omega \rightarrow \infty} P_{1,2} = \pm \frac{e^2\omega}{2c} \frac{1}{\gamma(t)^2\beta(t)} \quad (21)$$

and cancel exactly when summed. In a numerical evaluation, a small error remains, which grows linearly with  $\omega$ . Grouping the terms together prevents the growth of this error.

Under the assumptions that the electromagnetic fields vary slowly on the timescale of a photon formation length, and that linear acceleration emission (e.g. Schwinger 1949) is unimportant, we demonstrate in appendix A that (18) reduces to a local emissivity. This is an obvious generalization of standard synchrotron emission, which takes account of acceleration in both magnetic and electric fields by formulating it in terms of the local curvature of the trajectory:

$$P(\omega, t) = \frac{\sqrt{3}e^2\gamma\kappa}{2\pi} \frac{\omega}{\omega_c} \int_{\omega/\omega_c}^{\infty} dx K_{5/3}(x) \quad (22)$$

where

$$\omega_c = 3\gamma^3 c\kappa/2 \quad (23)$$

and the curvature  $\kappa$  is defined locally in terms of the particle velocity and acceleration  $\boldsymbol{\beta}$  and  $\dot{\boldsymbol{\beta}}$ :

$$\kappa = \frac{|\boldsymbol{\beta} \times \dot{\boldsymbol{\beta}}|}{c\beta^3} \quad (24)$$

A perturbative approach that includes linear acceleration emission as a first order correction to (22) has been presented by Melrose (1978).

To perform the integration in (18) numerically, we first split it at the points where  $\sin g = 0$ , i.e.,  $g = n\pi$ , ( $n = 0, \pm 1, \pm 2 \dots$ ), and write it as an infinite sum

$$P(\omega, t) = \frac{e^2\omega}{2\pi c} \sum_{n=-\infty}^{\infty} \int_{n\pi}^{(n+1)\pi} dg Q(g, t) \sin g \quad (25)$$

where

$$Q(g, t) = \frac{1}{g} \left\{ \left[ \frac{1}{\gamma^2(t)\beta(t)} \right] \left[ \frac{\beta(t)g}{\tau\dot{g} \left[ \beta(t) + \frac{\delta\Delta(t, \tau)}{|\tau|} \right]} - 1 \right] - \frac{g\boldsymbol{\beta}(t) \cdot \delta\boldsymbol{\beta}(t, \tau)}{\dot{g}\tau \left[ \beta(t) + \frac{\delta\Delta(t, \tau)}{|\tau|} \right]} \right\} \quad (26)$$

and  $\tau$  and  $\dot{g}$  are considered to be functions of  $g$  and  $t$ , defined implicitly in (16) and (20). According to its definition (4), integration from  $g = 0$  to  $g = 2\pi$  corresponds precisely to integration over one photon formation time. We therefore anticipate on physical grounds that taking the first few terms should give a good approximation. However, the function  $Q(g, t)$  grows linearly with  $g$  for small  $g$ , before decreasing monotonically above some critical value  $g^*$ . In this case, the sum in (25) does not begin to converge until  $n > n^* = g^*/\pi$ . For constant curvature, it is straightforward to show that  $g^* \approx 3\omega/\omega_c$ , so that  $n^*$  becomes large only if one tries to compute the emissivity well above the cut-off frequency. In general, we have found that a substantial improvement can be achieved by employing the Euler–van Wijngaarden transform (e.g. Press et al. 1986, section 5.1) to accelerate the convergence, whilst retaining a minimum number of about 20 terms in order to preserve accuracy at high frequencies, where the power radiated is low.

Evaluation of the instantaneous power based on (25) requires knowledge of the functions  $\beta(\tau)$  and  $\delta\Delta(\tau)$ . In the next section we apply this approach to finding the angular integrated emission of an isotropic, mono-energetic particle distribution in prescribed, stationary, turbulent fields, in which these functions can be found using an adjustable-step integration of the trajectory. In section 4, on the other hand, we discuss the application to a trajectory that is known only as a discrete time series, for example, a trajectory from a PIC simulation.

### 3. PRESCRIBED FIELDS

#### 3.1. Isotropic particle distribution

Equation (5) describes the energy emitted by a single particle. If we now consider the possibility of  $N$  particles emitting incoherently whilst following trajectories in a prescribed field in a volume  $V$ , and allow them to do so for a time  $T$ , then the average power  $L$  emitted by these particles is obtained by summing over the individual contributions:

$$\frac{dL}{d\omega} = \lim_{T \rightarrow \infty} \sum_{i=1}^N \frac{1}{T} \int_{-T/2}^{T/2} dt P_i(t) \quad (27)$$

where  $P_i(t)$  is the instantaneous power of the  $i$ 'th particle. Replacing the sum by an integral over the exact (Klimontovich) phase space distribution  $f_K(\mathbf{x}, \mathbf{p}, t) = \sum_{i=1}^N \delta[\mathbf{x} - \mathbf{x}_i(t)] \delta[\mathbf{p} - \mathbf{p}_i(t)]$  where  $\mathbf{x}_i(t), \mathbf{p}_i(t)$  are the phase-space coordinates of the  $i$ 'th particle at time  $t$ , leads to

$$\frac{dL}{d\omega} = \int d^3\mathbf{x} d^3\mathbf{p} \frac{1}{T} \int_{-T/2}^{T/2} dt f_K(\mathbf{x}, \mathbf{p}, t) P(\mathbf{x}, \mathbf{p}, t) \quad (28)$$

where  $P(\mathbf{x}_i(t), \mathbf{p}_i(t), t) = P_i(t)$ .

In general, both the electromagnetic fields that determine the particle trajectories and the phase space distribution fluctuate in time. However,  $L$  is a time-averaged quantity. If we are interested in the emission from a system containing prescribed, static fields, then  $P(\mathbf{x}, \mathbf{p}, t)$  is not an explicit function of time, so that

$$\frac{dL}{d\omega} = \int d^3\mathbf{x} d^3\mathbf{p} P(\mathbf{x}, \mathbf{p}) \frac{1}{T} \int_{-T/2}^{T/2} dt f_K(\mathbf{x}, \mathbf{p}, t) \quad (29)$$

If, in addition, we look at the radiation from a stationary coarse-grained particle distribution  $f(\mathbf{x}, \mathbf{p})$ , then, replacing the time-averaged Klimontovich function by this distribution leads to

$$\frac{dL}{d\omega} = \int d^3\mathbf{x} d^3\mathbf{p} P(\mathbf{x}, \mathbf{p}) f(\mathbf{x}, \mathbf{p}) \quad (30)$$

For the case of fluctuations in only the magnetic field, for example, the particle energy is an integral of motion, and any homogeneous, isotropic function of the Lorentz factor  $\gamma(p)$  is a stationary solution of the kinetic equation. Setting  $f(\mathbf{x}, \mathbf{p}) = \frac{N}{V} \frac{1}{4\pi p^2} \delta(\gamma - \gamma(p))$ , we find

$$\frac{dL}{d\omega} = \frac{N}{4\pi V} \int d^3\mathbf{x} d^2\Omega P(\mathbf{x}, p\Omega) \quad (31)$$

where  $\Omega = \mathbf{p}/p$ . Thus, in order to compute the power radiated per unit frequency interval, we must integrate the instantaneous power over all directions of the velocity vector at each point and over all positions within the source. In the following subsections we present computations of the radiation produced from an ensemble of relativistic particles in static turbulent magnetic field configurations, employing a Monte Carlo integration of Equation (31).

#### 3.2. Emission spectrum

The character of the radiation produced by a relativistic particle depends on whether the strength parameter

$$a = \frac{eF\lambda}{mc^2} \quad (32)$$

is greater than or less than unity, where  $\lambda$  is the typical size of the field structures and  $eF = \langle dp_{\perp}/dt \rangle$  the average transverse force on the particle (Landau & Lifshitz 1971). This Lorentz invariant parameter is analogous to the strength parameter commonly used in laser plasma physics, and is also sometimes called the ‘‘wiggler’’ or ‘‘undulator’’ parameter. For static fields, it determines roughly the ratio of the deflection angle to the beaming angle for a particle traversing a typical structure. For simplicity, electric fields are neglected for the remainder of this section ( $F = B_{\perp}$ ). Typically, the magnitude of the strength parameter determines whether the particle radiates in the synchrotron regime ( $a > 1$ ) or in the so-called jitter/diffuse synchrotron regime ( $a < 1$ ).

For a given  $B_{\perp}$  and  $\lambda$ , the maximum photon energy can be determined. However, the full details of the spectrum produced by a particle, even in a relatively simple field configuration, can be quite complicated. Using the algorithm presented in the previous section, the equations of motion can be integrated simultaneously with equation (25), providing the complete spectrum. For the results that follow a fifth-order adaptive Runge-Kutta integrator was used (Press et al. 1986). With the aid of some illustrative examples, we demonstrate how different spectral features can be produced, and emphasize the properties of the fields required to do so.

#### 3.3. Uniform fields – the synchrotron approximation

As a first example, the radiation produced from a particle gyrating in a uniform field is compared to the analytic solution for synchrotron radiation, Eq. (22). The results



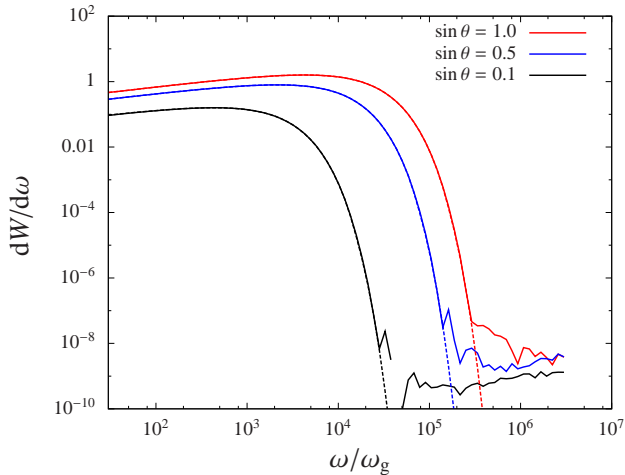


FIG. 1.— Instantaneous power spectrum produced by a particle of Lorentz factor  $\gamma = 10^2$  with different pitch angles in a uniform magnetic field  $\mathbf{B}$ , as a function of angular frequency in units of  $\omega_g = eB/mc$ , with  $\theta$  the angle between the particle velocity and the field. The numerical values (solid lines) are in excellent agreement with the instantaneous synchrotron approximation (dashed lines). The noise at high frequencies can be controlled by increasing both the number of terms taken in the series and the integrator accuracy.

are shown in Fig. 1 and are in excellent agreement with the analytic result. At very high frequencies, the formation lengths become extremely short, and  $Q$  can be linear in  $g$  for several periods. Errors in the particle integrator can also become an issue. For the results shown in Fig. 1 a fractional error control of  $10^{-7}$  was used and the power was summed from  $n = 0$  to  $n = \pm 10$ . As discussed in section 2.1, the series fails to converge if  $n^* > 10$ . However, this occurs only well above the cut-off frequency. As we discuss in section 4, when dealing with discrete time series, the “synchrotron approximation” must be taken at high frequencies, where the formation length is small.

The grouping of the terms described in Equation (18) is vital in keeping the high frequency noise below the integrator accuracy. This is also important for calculations in turbulent fields when there is a large variation in the roll-over frequency of the instantaneous power. Provided the high frequency noise remains below the threshold, the results are reliable.

### 3.4. Turbulent fields

In a turbulent magnetic field, the particle trajectory and resulting radiation spectrum are generally quite complex (Toptygin & Fleishman 1987). Nevertheless, several qualitative features can be understood in terms of the strength parameter, although the product  $B\lambda$  is replaced by a different value for each Fourier mode. There is now no single strength parameter but rather a spectrum  $a(k) = 2\pi eB(k)/(mc^2k)$ , and radiation produced depends on several factors, most notably the turbulent spectrum and the magnitudes of  $a(k_{\min})$  and  $a(k_{\max})$ .

To investigate the effect of different turbulent field parameters, static fields are constructed with the required properties. This is done using a discrete Fourier transform description following the method of Giacalone & Jokipii (1999). The magnetic field at a position  $\mathbf{x}$  is  $\mathbf{B}(\mathbf{x}) = \mathbf{B}_0 + \delta\mathbf{B}(\mathbf{x})$ , where  $\mathbf{B}_0$  represents an external uniform mean field. The turbulent field component is generated using  $N$  Fourier modes, each with a

random phase, direction and polarization. In the limit of large  $N$ ,

$$\delta\mathbf{B}(\mathbf{x}) = \lim_{N \rightarrow \infty} \sum_{n=1}^N A_n e^{i(\mathbf{k}_n \cdot \mathbf{x} + \beta_n)} \hat{\xi}_n \quad (33)$$

represents an isotropic turbulent field. Here  $A_n$ ,  $\beta_n$ ,  $\mathbf{k}_n$  and  $\hat{\xi}_n$  are the amplitude, phase, wave vector and polarization vector for each mode  $n$  respectively. The polarization vector is determined by a single angle  $0 < \psi_n < 2\pi$

$$\hat{\xi}_n = \cos \psi_n \mathbf{e}_x + i \sin \psi_n \mathbf{e}_y \quad (34)$$

where  $\mathbf{e}_x$  and  $\mathbf{e}_y$  are vectors, orthonormal to  $\mathbf{e}_z \equiv \mathbf{k}_n/k_n$ . The vector  $\mathbf{k}_n$  is determined by two additional angles,  $0 < \theta_n < \pi$  and  $0 < \phi_n < 2\pi$ , and, for an isotropic distribution, should be uniformly distributed on the unit sphere. These two angles define a rotation matrix that determines  $\mathbf{e}_x$  and  $\mathbf{e}_y$  (e.g. Giacalone & Jokipii 1999).

The amplitude of each mode is

$$A_n^2 = \sigma^2 G_n \left[ \sum_{n=1}^N G_n \right]^{-1}$$

where the variance  $\sigma^2$  is chosen such that the turbulent field is normalized to give the required turbulence level:

$$\eta = \frac{\langle \delta B^2 \rangle}{B_0^2 + \langle \delta B^2 \rangle} \quad (35)$$

We use the following form for the power spectrum

$$G_n = \frac{\Delta V_n}{1 + (k_n L_c)^\alpha} \quad (36)$$

where  $L_c$  is the correlation length of the field and  $\alpha$  is the asymptotic spectral index of the turbulence spectrum. For the three-dimensional fields used in this paper the normalization factor is  $\Delta V_n = 4\pi k_n^2 \Delta k_n$ , and the  $\Delta k_n$  are chosen such that there is equal spacing in logarithmic  $k$ -space, over the finite interval  $k_{\min} \leq k \leq k_{\max}$ . For a detailed discussion of the statistical properties of fields constructed in this manner see Casse et al. (2002). The field can be constructed at any point in space by summing over the  $N$  modes, providing an infinite spatial description of the fields. This avoids the need for boundary conditions. The parameters used for each field construction are given in Table 1.

The spectra are produced using a Monte Carlo integration of Equation (31). At each frequency  $\omega$  a sample particle of fixed Lorentz factor is placed at a random location  $\mathbf{x}_i$  inside a volume with dimensions several times the size of the correlation length,  $L_c$ , of the turbulent field. To represent an isotropic particle distribution, the particle is given a random initial direction  $\Omega_i$ , and the instantaneous power  $P_i$  is calculated. The average power emitted per particle at each frequency is determined using a Monte Carlo integration:

$$\begin{aligned} \frac{dW}{d\omega} &= \frac{1}{4\pi V} \int_V d^3\mathbf{x} \int d^2\Omega P(\mathbf{x}, p\Omega) \\ &\approx \frac{1}{n} \sum_{i=1}^n P_i \end{aligned} \quad (37)$$

TABLE 1  
TURBULENT FIELD PARAMETERS

Field	$B_{\text{rms}}$	$2\pi/k_{\text{max}}$	$2\pi/k_{\text{min}}$	$L_c$	$\eta$	$\alpha$
A	1.0	2	160	80	1.0	11/3
B	1.0	2	320	160	1.0	11/3
C	0.05	0.5	10	5	1.0	11/3
D	1.0	0.05	10	5	1.0	8/3
E	0.1	0.1	1	0.5	1.0	9/3
F	1.0	0.05	10	5	0.1	8/3
G	1.0	0.1	10	5	0.9	8/3

NOTE. — Parameters used in the field constructions for turbulent field spectra. All quantities are dimensionless, with the magnetic field in units of an arbitrary normalization value  $B_0$ . All length scales are in units of  $mc^2/eB_0$ . The maximum strength parameter in each run is given approximately by the product  $2\pi B_{\text{rms}}/k_{\text{min}}$ .

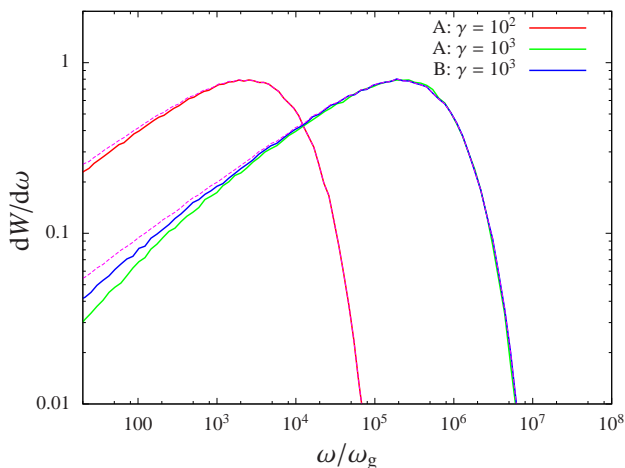


FIG. 2.— Radiation spectra for an isotropic distribution of monoenergetic particles in a fully turbulent field with strength parameter  $a \gg 1$ , as a function of frequency in units of  $\omega_g = eB_0/mc$ .  $dW/d\omega$  represents the average power emitted by each particle and is plotted in units  $e^2\omega_g/2\pi c$ . The dashed lines show the integral of the instantaneous power, evaluated in the synchrotron approximation.

The number of integration points  $n$  is determined from the condition that the standard deviation error estimate is well below than 10%. This usually requires only a relatively small number of points at low frequencies. However, if  $a(k_{\text{max}}) \ll 1$ , a large number of points is needed at high frequencies in order for the Monte Carlo integrator to resolve these small scale structures. For comparison, the instantaneous synchrotron power, Equation (22), is also calculated at each point.

Figures 2 – 4 show the spectra produced by an isotropic homogeneous particle distribution in turbulent isotropic fields with zero mean field component. A common feature of each of these spectra is a hardening at low frequencies. This arises because the particle begins to be deflected by the turbulence through an angle comparable to that of the beaming cone of the radiation, whilst traversing a photon formation length, which grows towards low frequency. If the particle motion can be described as diffusion in the (small) angle  $\theta$  between its velocity vector and a suitably chosen coordinate axis, this is known as the Landau-Pomeranchuk-Migdal (LPM) effect (Landau & Pomeranchuk 1953a,b; Migdal 1956) — a well-studied phenomenon in the context of the sup-

pression of bremsstrahlung and pair-production in crystals and other media (for a review see Klein 1999), though not usually considered in the context of synchrotron radiation (although see Toptygin & Fleishman 1987; Fleishman 2006b). The effect can be understood as follows: For a trajectory with constant curvature  $\kappa$ , and constant acceleration,  $\dot{\beta} = 0$ , the particle displacement is  $\Delta \approx \beta\tau - c^2\kappa^2\tau^3/24$  (see equation A8). For low frequencies the resulting formation length is dominated by the  $\tau^3$  term. It is this scaling that gives synchrotron radiation its  $\omega^{1/3}$  asymptote at low frequencies. However, in turbulent fields, both the acceleration and curvature vary. Thus, at low frequencies, when the formation lengths are long, a particle can undergo multiple scattering within a formation time. In general, for small angle scattering ( $a \ll \gamma$ ), the displacement is  $\Delta \approx \beta\tau - \frac{1}{2}\int_0^\tau dt\theta^2(t) + \frac{1}{2\tau}(\int_0^\tau dt\theta(t))^2$ , and the spectrum should be averaged over a large ensemble of particles (e.g. Landau & Pomeranchuk 1953a; Akhiezer & Shul'ga 1987). For pitch-angle diffusion, i.e.  $\langle\theta\rangle = 0$  and  $\langle\theta^2\rangle \propto t$ , the average displacement is proportional to  $\tau^2$  at low frequencies, resulting in an  $\omega^{1/2}$  spectrum. However, the transition to this regime requires many scatterings and may not be realized within a formation length in a specific realization of a turbulent field.

This is illustrated by the examples described in the following subsections. The radiation spectra produced in these examples can be placed into three broad categories, corresponding to the two extreme cases where  $a(k_{\text{min}}) \gg 1$  or  $a(k_{\text{min}}) \ll 1$  and an intermediate range in which  $a(k_{\text{min}})$  is of order unity.

### 3.4.1. $a(k_{\text{min}}) \gg 1$

In the case of large strength parameters, since the particle in general sweeps through an angle larger than its beaming angle, the spectrum should resemble that of the instantaneous synchrotron spectrum close to the critical frequency. Fig. 2 shows the resulting spectrum for two different field configurations. As expected, the spectrum matches very closely that of the instantaneous synchrotron approximation in the vicinity of the roll-over frequency. Below this value, the numerically determined spectrum diverges slowly from the instantaneous synchrotron line, becoming gradually harder at lower frequencies. Note that in the large strength parameter regime, the transition to the diffusive LPM regime described above, i.e. the  $\omega^{1/2}$  scaling, should occur when the formation length exceeds the longest wavelength in the system, which occurs only at very low frequencies  $\omega \sim \omega_c/a(k_{\text{min}})^3$ . The divergence from the synchrotron spectrum follows from Equation (A8) since now both  $\dot{\kappa}$  and  $\dot{\beta}$  are non-zero, and the coefficient of the  $\tau^3$  term will have an additional time-dependence. For the range of frequencies considered, the spectrum does not approach a low-frequency power-law asymptote, but continues to harden gradually as it approaches  $\omega_g$ , where the synchrotron approximation fails and the beaming cone is large. The smaller the value of  $a(k_{\text{min}})$  the more rapidly the spectrum diverges from that of the instantaneous synchrotron approximation. The spectra are not sensitive to the value of  $a(k_{\text{max}})$  in the  $a(k_{\text{min}}) \gg 1$  regime, provided  $a(k_{\text{max}}) \ll 1$ .

For frequencies above the roll-over frequency, as can be seen in Fig. 2, the spectrum is in excellent agreement with the instantaneous synchrotron approximation. On physical grounds it is expected that a power-law tail must occur at higher frequencies due to the high frequency jittering resulting from modes with  $a(k) < 1$  (see e.g. Fleishman 2006c). However, for the turbulent spectra considered, the power associated with such fluctuations is extremely small, and the numerical accuracy required to resolve such a feature in the large  $a(k_{\min})$  regime is beyond the capabilities of current computational resources.

#### 3.4.2. $a(k_{\min}) \ll 1$

For fields composed exclusively of small strength parameter fluctuations, the particle deflections are small and, at sufficiently high frequencies, it is possible to use standard perturbation techniques (Landau & Lifshitz 1971; Medvedev 2000; Fleishman 2006b). Numerically, this regime is far more challenging since the time steps in the integrator must resolve deflections in the particle's trajectory on the order  $a(k_{\max})/\gamma$ . Figs. 3 and 4 show the spectra produced in fields with  $a(k_{\min}) = 0.5$  and  $a(k_{\min}) = 0.1$  respectively. Both spectra exhibit a break at the critical frequency  $\omega \approx \gamma^2 k_{\min} c$ . Above this frequency, the spectrum has a power-law slope matching that of the turbulence spectrum. This can be understood as the up-scattering of the virtual photons of the field by the mono-energetic particles. In principle, the power law should extend up to  $\omega \approx \gamma^2 k_{\max} c$ , however, the numerical accuracy of the integrator chosen for this example is insufficient to display the entire range. At even higher frequencies,  $\omega \gg \gamma^2 k_{\max} c$  the fields are constant over the formation length of the particle, and the instantaneous synchrotron approximation applies. As we discuss in section 4, if the formation length of a particle is not well resolved, it is exactly in this regime that the instantaneous synchrotron approximation must be used. Below the critical frequency, the photon formation time remains short compared to the time taken to deflect through an angle greater than  $\gamma^{-1}$ . The displacement is approximately  $\Delta \approx \beta \tau$  and, as in the case of relativistic bremsstrahlung, the spectrum is approximately flat  $dW/d\omega \propto \omega^0$ . Ultimately, at frequencies  $\omega < a(k_{\min})\omega_c \approx a(k_{\min})^2 \gamma^2 c k_{\min}$ , the formation time exceeds the time needed to diffuse out of the beaming cone and the spectrum is determined by the LPM effect (Fleishman 2006b).

#### 3.4.3. $a(k_{\min}) \sim 1$

The intermediate range where the value of  $a(k_{\min})$  is somewhat larger than unity, is interesting because it emerges from PIC simulations of Weibel mediated shocks (e.g. Sironi & Spitkovsky 2009b). An example of the spectrum produced in such a field is shown in Fig. 5. For this example, the strength parameter  $a(k_{\min})$  is of order unity, and the transition to the LPM regime occurs at relatively high frequencies, close to the roll-over frequency. However, above the roll-over frequency, unlike in the  $a(k_{\min}) \gg 1$  regime, the small strength parameter modes can be resolved, and similar to the  $a(k_{\min}) \ll 1$  spectra, a high frequency power-law emerges. The shape of the power-law matches that of the turbulence spectrum. This presents a possible observational signature of short wavelength turbulence at relativistic shocks. The presence of such short wavelength turbulence is supported

by current PIC simulations in which Fermi acceleration is found to occur.

#### 3.4.4. *Non-zero mean field*

In general, the radiation spectrum can be affected if the mean field is non-zero or if turbulence is generated on different scales such that the large scale fluctuations act as a local mean field. The latter situation could in principle be realized in the presence of large scale MHD turbulence produced from interaction between the shock front and density inhomogeneities (e.g. Sironi & Goodman 2007) and short wavelength turbulence produced via kinetic effects in the shock transition region. In the presence of two populations of scatterers, if they are generated on very different length-scales, it is possible for the synchrotron radiation of shock-accelerated particles to extend into the gamma-ray range, whereas for a single population of scatterers radiation losses restrict it to relatively low frequency (Kirk & Reville 2010).

Here we consider the radiation produced in a region with a mean field having a superimposed turbulence spectrum. If the energy in the turbulent fluctuations is negligible with respect to the total field,  $\eta \ll 1$ , where  $\eta$  is defined in (35), the low frequency spectrum will match that of the instantaneous synchrotron spectrum, since scattering will be ineffective, and to zeroth order, the particles simply gyrate about the mean field. At higher frequencies, provided modes with  $a < 1$  exist, a power-law tail can emerge. Again, depending on the power associated with these modes, the numerical scheme can capture this feature, provided it is not too deep in the exponential cut-off region. To illustrate this, we show in Figure 6 the spectra produced in turbulent fields, with modest maximum strength parameters, and different values of  $\eta$ . For small  $\eta$ , i.e. weak turbulence, the spectrum reproduces that of the instantaneous synchrotron spectrum, although a high frequency tail is also produced, due to the fluctuations on modes with  $a < 1$ . As  $\eta$  increases, more power goes into the high frequency emission, and a reduction in the power at low frequencies is observed, although for the frequencies investigated, the spectrum maintains a  $\omega^{1/3}$  scaling.

As the ratio of the energy density in the turbulent field to that of the total field is increased further, we return to the previously investigated regimes. For example, in a Weibel mediated shock  $1 - \eta \ll 1$  (Sironi & Spitkovsky 2009a). However, to investigate clearly identifiable signatures, it is necessary to move beyond the prescribed, homogeneous turbulent fields considered here to more self-consistent realizations, resulting from the simulations.

## 4. TRAJECTORIES AND FIELDS GIVEN AS A TIME SERIES

A PIC simulation is capable of producing a large number of time series listing the position and velocity of the simulation particles and the values of the electromagnetic fields at each time-step. Using these, it is possible to produce spectra and light curves. The synthetic spectra presented in section 3 are based on isotropic mono-energetic particle distributions as described in section 3.1. In general, however, the particle distribution is not only energy dependent, but can be highly anisotropic. This can in principal be studied by numerically solving

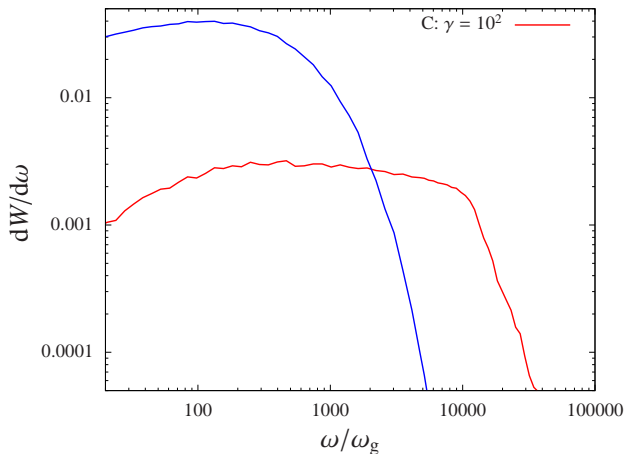


FIG. 3.— Radiation spectra for an isotropic distribution of particles in a fully turbulent field with all strength parameters  $a < 1$ . The blue line is the integrated instantaneous synchrotron spectra. The high frequency asymptote is close to the shape of the turbulent spectrum  $\propto \omega^{-11/3}$ . The low frequency spectrum does not converge to a power law for the range of frequencies considered.

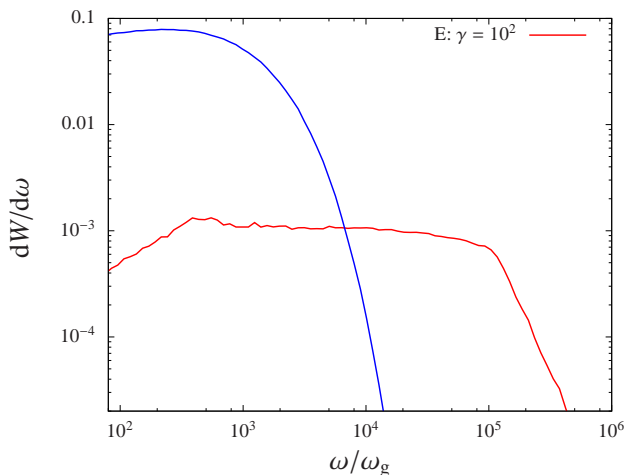


FIG. 4.— Radiation spectra for an isotropic distribution of particles in a fully turbulent field with strength parameters  $a < 1$  using a smaller value for  $a(k_{\min})$  and a larger dynamic range than in Fig. 3. The blue line is the integrated instantaneous synchrotron spectra. The high frequency asymptote is close to the shape of the turbulent spectrum  $\propto \omega^{-3}$ . The low frequency spectrum has a spectral slope  $\sim 0.7$ .

Equation (1) or Equations (2) and (3) for each trajectory, and then summing over trajectories, which is equivalent to integrating over the particle distribution function. However, the radiation from an individual trajectory is beamed into an opening angle  $\sim 1/\gamma$ . If this is smaller than the scales on which the particle distribution is anisotropic, the order of these operations can be reversed (see Ginzburg & Syrovatskii 1965, section 3.2). The average over the particle distribution is then replaced by an integration over angles of the radiation emitted by a single trajectory (which can be performed analytically), and the radiation observed in a given virtual detector is given by summing over all those trajectories whose velocity vector lies within the acceptance cone

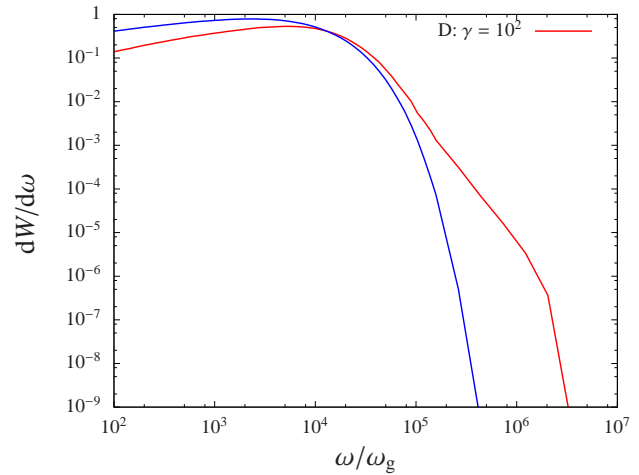


FIG. 5.— Radiation spectra for an isotropic distribution of particles in a fully turbulent field with strength parameter  $a(k_{\min}) \gtrsim 1$  and  $a(k_{\max}) \ll 1$ . The blue line is the integrated instantaneous synchrotron spectra. The index of the high frequency power-law component is close to that of the turbulent spectrum  $\propto \omega^{-8/3}$ . Evidence of a cut-off is observed close to where the formation length  $L_c \sim 1/k_{\max}$ , where the line must match up with the instantaneous synchrotron approximation. This cannot be resolved numerically.

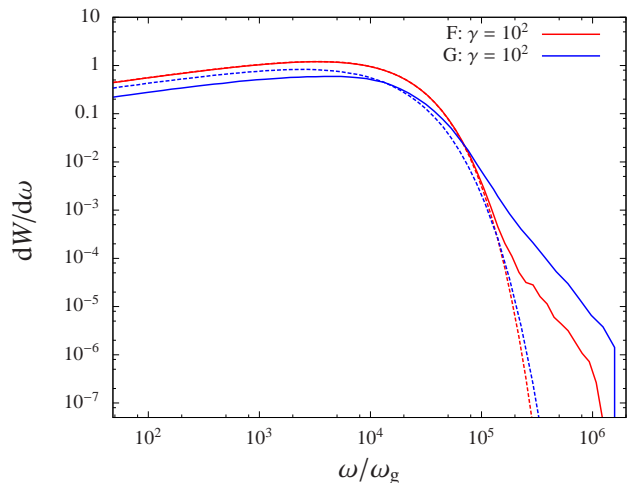


FIG. 6.— Spectra emitted in the presence of a finite mean field  $\eta = 0.1$  (red curves) and  $\eta = 0.9$  (blue curves), where  $\eta$  is the ratio of the energy density in the turbulent field to the total energy density – see (35). The instantaneous synchrotron spectra are plotted using dashed lines. The total energy density in the magnetic field is fixed, so that the magnitude of the average field differs in the two cases. As in Fig. 5, there is evidence of a cut-off at high frequencies.

of that detector. Formally,

$$\begin{aligned} \frac{dL}{d\omega d\mathbf{n}} &= \int d^3\mathbf{x} dp p^2 d^2\Omega f(\mathbf{x}, p\mathbf{n}, t) P(\mathbf{n}, \omega, t) \\ &\approx \int d^3\mathbf{x} dp p^2 f(\mathbf{x}, p\mathbf{n}, t) \int d^2\Omega P(\Omega, \omega, t) \\ &= \int d^3\mathbf{x} dp p^2 f(\mathbf{x}, p\mathbf{n}, t) P(\omega, t) \end{aligned} \quad (38)$$

and the integrations over  $\mathbf{x}$  and  $p$  reduce in the PIC case to summations over all trajectories that illuminate the specified detector.

For the high-energy emission of particles accelerated at



a relativistic shock front, the restriction imposed by this procedure is not important, because the anisotropy of the particle distribution is expected to be on a scale larger than the beaming angle. Thus, the angular dependence of the emitted radiation found by Sironi & Spitkovsky (2009b) and Frederiksen et al. (2010) should just reflect the angular dependence of the distribution function at the relevant particle energy, and would be preserved in this approach.

As pointed out by Hededal (2005) the computation of synthetic spectra from trajectories taken from PIC simulations inevitably involves interpolation. Specifically, the algorithm presented in (9)–(11) transforms the integration variable from time to phase. In order to split the contributions to the integral into an alternating series (25), the discrete trajectory must be interpolated.

Interpolation is not a sensitive procedure provided many points are contained within a photon formation time, a constraint that will be made more precise below. An accurate evaluation of the instantaneous power at any time step can, for example, be obtained simply by linearly interpolating the functions  $g$ ,  $\gamma$ ,  $\beta$ ,  $\dot{g}$ ,  $\delta\beta$  and  $\delta\Delta$ , which are known at all neighboring grid points. When the photon formation length drops to only a few time steps, this procedure fails. However, the validity of the PIC simulation requires that the electromagnetic fields vary slowly between time steps, which is precisely the condition for applicability of the generalized synchrotron formula (22). Therefore, in a valid simulation, the instantaneous power can safely be evaluated using this method, if the formation time is not long compared to the time step. It follows that, for a given frequency, the method of evaluating the instantaneous power at each of the discrete set of particle positions  $\mathbf{x}(t_n)$ , depends on the value of the photon formation time at that point.

At high frequencies, the formation time is short, and can be much shorter than the typical time-step used in PIC simulations, which is a fraction of a plasma cycle. It is straightforward to find for each time-step (labeled by  $n$ ) the values  $\delta\Delta_n^\pm$  of the deviation of the displacement at the neighboring points  $n \pm 1$ . For a given frequency, the photon formation lengths in the forward and backward directions follow. Alternatively, two critical frequencies  $\omega_n^\pm$  can be found such that at these frequencies the neighboring points lie precisely one formation length away from  $x_n$ . From Equations (4) and (14) the critical frequencies are

$$\omega_n^\pm = \frac{4\pi\gamma^2}{\delta t_n^\pm + 2\gamma^2|\delta\Delta_n^\pm|} \quad (39)$$

where  $\delta t_n^\pm = |t_{n\pm 1} - t_n|$  is the time-step between neighboring data points. If  $\omega$  is close to or greater than  $\omega_n^\pm$ , then the coherence length is poorly resolved and the synchrotron approximation must be used to compute the instantaneous power. If, on the other hand,  $\omega \ll \omega_n^\pm$ , then the coherence length is well resolved, and a numerical integration is accurate.

The accuracy of the solution depends quite strongly on the ability to resolve the peaks and troughs of the sine function in Equation (25). PIC simulations usually work with a fixed time-step, in which case the resolution in successive terms in (25) decreases. This case be seen by considering the time evolution of the phase. Making a

Taylor expansion about the initial position gives

$$g \approx \omega \left[ \frac{\tau}{2\gamma^2} + \frac{1}{24}c^2\beta^3\kappa^2\tau^3 \right] \quad (40)$$

For  $\tau > 3/\gamma\kappa$ , the  $\tau^3$  term dominates and one can solve for  $g = n\pi$  to give

$$\tau_n \approx \frac{\gamma^2}{\omega_c} \left( 54n\pi \frac{\omega_c}{\omega} \right)^{1/3} \quad (41)$$

It is readily seen that for larger  $n$  the time interval between successive integer multiples of the phase  $g = n\pi$  decreases:

$$\tau_{n+1} - \tau_n \approx \frac{\gamma^2}{\omega_c} \left( \frac{2\pi}{n^2} \frac{\omega_c}{\omega} \right)^{1/3} \quad (42)$$

For this reason, it is essential to interpolate the functions  $Q$  and  $g$ , rather than the combination  $Q \sin g$ , and we have found that linear interpolation is adequate. Then, trapezoidal integration in the phase  $g$  is used with a maximum step-size of  $\Delta g = 2\pi/25^1$  to evaluate the terms  $n = -10 \dots 10$  in (4).

As an illustrative example, we again consider the case of uniform circular motion. In Fig 7 we plot the energy radiated per frequency interval over one gyration. In addition to the analytic solution, the result of integrating the instantaneous power calculated using various time-steps is shown. In this special example, both the instantaneous power and the frequencies  $\omega_n^\pm$  are independent of time, so that use of the synchrotron approximation automatically yields the exact analytic result. The numerically determined power reproduces this result to within 1% for frequencies

$$\omega < \frac{1}{25} \text{Min}(\omega_n^+, \omega_n^-) . \quad (43)$$

At higher frequencies, the instantaneous power itself may still be evaluated accurately, since the interpolation scheme guarantees 25 points per photon formation length. However, since this quantity is evaluated only at each time-step, the subsequent integration required to evaluate the radiated energy does not reach the required resolution.

This suggests the following procedure when the algorithm is employed in an arbitrary field configuration: The frequency at which the emission is to be evaluated, is compared at each time-step to the frequencies  $\omega_n^\pm$ . If  $\omega$  satisfies the inequality (43), numerical integration is used. Otherwise, the instantaneous synchrotron expression (22) is used.

An important property of this algorithm is that it avoids explicitly interpolating the particle's position and velocity. Such a procedure introduces discontinuities into the particle acceleration as a function of time, leading to high-frequency artifacts similar to those that arise when the acceleration of a hyperbolic trajectory is abruptly terminated (Reville & Kirk 2010).

As mentioned above, the instantaneous power can only be evaluated accurately by integrating over at least the

<sup>1</sup> This is approximately the resolution required to calculate  $\int_a^b \sin(x)dx$  to better than 99% accuracy using trapezoidal integration.

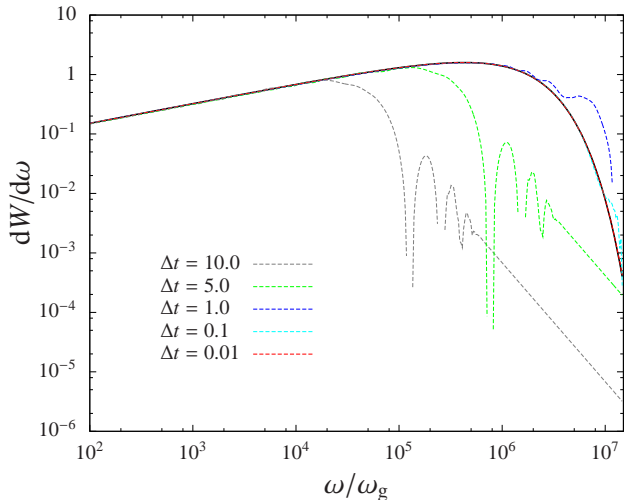


FIG. 7.— Synchrotron spectra found using discrete time-series data for a  $\gamma = 10^3$  particle using linear interpolation on  $Q$  and  $g$  between data points, for a range of time-step sizes (in units of  $\omega_g^{-1}$ ). In each case, the frequency at which the numerical result begins to deviate from the exact answer is in close agreement with (43).

first few formation lengths. The number of terms needed in (25) can be considerably reduced with the aid of the Euler–van Wijngaarden transform. However, when calculating the total energy spectrum radiated by an individual trajectory, it is also essential to resolve the instantaneous power as a function of time. Given a finite time series of positions and velocities, the radiation formulas apply only if the trajectory is extrapolated ballistically outside of the finite length time series, although the behavior in these regions does not affect the results when frequencies  $\omega \gg \langle \gamma^2 \rangle / T$  are considered. Here  $\langle \gamma^2 \rangle$  is the average Lorentz factor squared along the trajectory, and  $T$  the total time. Of course, if a time-dependent light-curve is to be generated, the restriction is much more severe, since then  $T$  refers to the time-interval between successive evaluations.

To illustrate this, we consider the spectrum produced by a relativistic particle that undergoes an instantaneous scattering at  $t = 0$  through an angle  $\alpha$ . The spectrum in this case is well known to be flat,  $\omega^0$ , at frequencies small compared to the inverse duration of the acceleration (for a detailed discussion see Schwinger et al. 1998, chapter 37). The angular integrated spectrum in this frequency range can be determined analytically (e.g. Akhiezer & Shul’ga 1987)

$$\frac{dE}{d\omega} = \frac{2e^2}{\pi c} \left[ \frac{2\xi^2 + 1}{\xi \sqrt{\xi^2 + 1}} \ln |\xi + \sqrt{\xi^2 + 1}| - 1 \right] \quad (44)$$

Although this example appears straightforward, it is, in fact, quite demanding numerically, the reason for this being that the instantaneous power is itself an oscillatory function. The formation length at any given time  $t$  can be easily calculated, but the exact expression is cumbersome. Far from the scattering center,  $t_c = 4\pi\gamma^2/\omega$ . As the scatterer is approached, the formation length decreases, reaching a minimum at  $t = 0$ , of

$$l_c = ct_c \approx \frac{4\pi\gamma^2 c}{\omega(1 + 4\xi^2)} \quad (45)$$

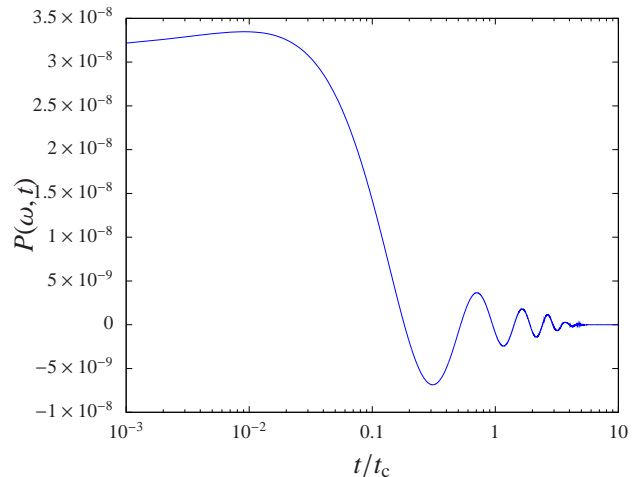


FIG. 8.— Instantaneous power at frequency  $\omega = 1$  (in arbitrary dimensionless units) as a function of time produced by a particle with  $\gamma = 10^3$  that undergoes an instantaneous scattering at  $t = 0$  through an angle  $\alpha = 2 \times 10^{-4}$  ( $\xi = 0.1$ ). Time is measured in units of the coherence time given by Eq. (45).

In this example there is no intrinsic time scale, so that we are free to choose arbitrary time, distance and frequency units. Defining a reference time unit  $t_0$ , we construct dimensionless units  $\hat{t} = t/t_0$ ,  $\hat{x} = x/ct_0$  and  $\hat{\omega} = \omega t_0$ .

Figures 8 and 9 show the instantaneous power as a function of time for  $\xi = 0.1$  and  $\xi = 10$ , respectively. The power oscillates with a slowly increasing period approximately equal to the formation time and damping with distance from the scatterer. In addition, there is an unresolved discontinuity at  $t = 0$ , which arises because the particle velocity is also discontinuous at this point. However, after integration over  $t$ , this feature has no influence on the energy radiated. Clearly, the linear growth phase for  $Q(g, t)$  will increase with distance from the scattering event, and the number of terms in the Euler–van Wijngaarden transform should be chosen such that the scattering is included. However, since the dominant contribution to the total energy radiated comes from the first few periods, the integral of the instantaneous power converges rapidly and the error incurred from taking only the first few formation lengths when calculating  $P(\omega, t)$  is small.

To demonstrate the effects of having a finite trajectory, we integrate the instantaneous power over a time interval

$$\frac{dE}{d\omega} = \int_{-T}^T P(\omega, t) dt$$

with  $T = \pi\gamma^2/(1 + 4\xi^2)$ , corresponding to one formation length for an emitted wave with frequency  $\omega = 4$ . From figures 8 and 9, it is clear that the solution will converge only for frequencies much larger than this. The instantaneous power is integrated using a finite time step trapezoidal integration for two different scattering angles  $\xi = 0.1$  and  $\xi = 10$ , with  $\gamma = 10^3$ , as above. The results are shown in figure 10. The result is in good agreement with the analytic solution above approximately  $\omega = 20$ . This suggests that for a given trajectory, on a time interval  $[-T, T]$ , the minimum frequency that can be investigated must have at least 10 formation lengths in this time interval.

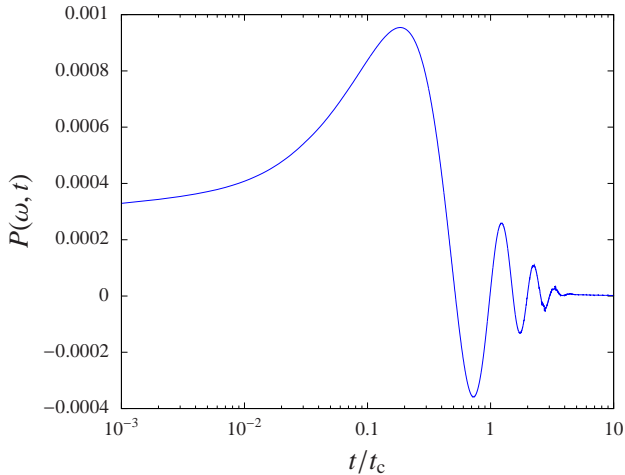


FIG. 9.— Instantaneous power at frequency  $\omega = 1$  as a function of time produced by a particle with  $\gamma = 10^3$  that undergoes an instantaneous scattering at  $t = 0$  through an angle  $\alpha = 2 \times 10^{-2}$  ( $\xi = 10$ ). Time is measured in units of the coherence time given by Eq. (45).

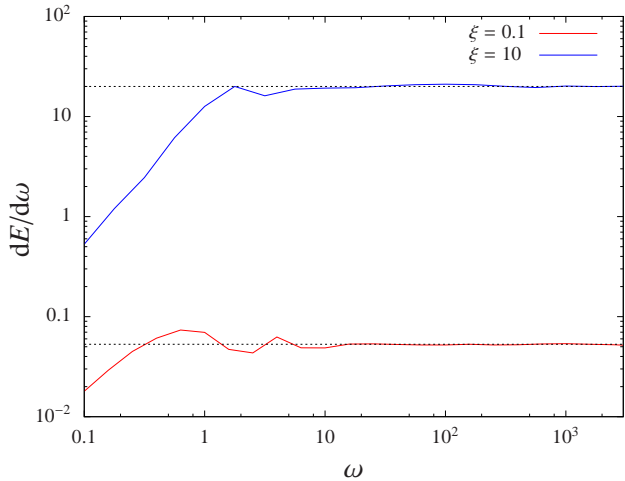


FIG. 10.— Plot demonstrating the low frequency limitation due to finite endpoints of the trajectory. The dashed line is the analytic result from (44). For the numerical evaluation, the instantaneous power was evaluated on the time interval  $-T < t < T$  where  $T = \pi\gamma^2/(1 + 4\xi^2)$  with  $\gamma = 10^3$  and  $\xi = 0.1$  and  $\xi = 10$ .

## 5. DISCUSSION

In this paper we describe an algorithm for calculating the radiation emitted by a relativistic charged particle moving in turbulent electromagnetic fields, and use it to investigate the spectra that arise in a prescribed, stochastic realization of a static, turbulent magnetic field. We also describe how to adapt the approach when the trajectory is given as finite time series for the position, velocity and acceleration. The algorithm is based on formulating an “instantaneous power” at each point on the trajectory, and makes use of the concept of the photon formation length to evaluate this quantity. It is suitable for use in post-processing the output from a particle-in-cell simulation.

Two problems arise with a numerical evaluation of the radiation. At high frequencies, the finite time-resolution of the trajectory is a limitation. For relativistic particles, this problem can be alleviated by suitable grouping of the terms associated with the slowly and rapidly varying

components of the instantaneous power, which improves the stability and accuracy. But even with the appropriate grouping of the terms, if the time-resolution of the trajectory cannot be improved indefinitely, a purely numerical evaluation still fails at sufficiently high frequency. Fortunately, it is precisely in this range that the instantaneous power can safely be evaluated using the synchrotron approximation. Subsequent integration of this quantity does not present a difficulty. However, for non-relativistic particles, or for frequencies comparable to the instantaneous angular frequency of the emitting particle, additional terms enter into the expression for the instantaneous power (15)

At low frequencies, a limitation is imposed when the trajectory is known only within a finite time interval. This intrinsic restriction cannot be removed: the minimum frequency at which a light curve can be computed is roughly  $10\gamma^2/T$ , where  $T$  is the length of the available time series. In current PIC simulations, however, the neglect of the collective response of the plasma to the propagating waves, which leads to effects such as Razin-Tsytovich suppression and transition radiation, is also likely to be important. These should intervene at frequencies below roughly  $\sim \gamma\omega_p$ , where  $\omega_p = \sqrt{4\pi n e^2/m}$  is the plasma frequency and  $n$  the number density, but to date it does not appear feasible to account for such effects self-consistently. For particles of Lorentz factor 100, these estimates imply that the intrinsic restriction is more important than the neglect of collective effects only when time-series shorter than about  $10^3$  plasma cycles are used to compute the emitted radiation.

Our results obtained for 3D magnetostatic turbulence confirm that one observational signature of short length-scale turbulence, is the presence of a high-frequency power-law tail in the mono-energetic emission spectrum Fleishman (2006a). For a power law of electrons  $dn/d\gamma \propto \gamma^{-p}$ , one expects a synchrotron power-law spectrum  $F_\omega \propto \omega^{-s}$ , where  $s = (p - 1)/2$ , for frequencies below the roll-over frequency of the maximum energy electrons. Observations of GRBs place this index in the range  $2 < p < 2.8$ , corresponding to a spectral index of  $0.5 < s < 0.9$ . Thus, unless the turbulence index is extremely hard,  $\alpha < 1$ , the photon spectrum will not harden at high frequencies, and this observational signature may be difficult to distinguish from a cut-off.

The synchrotron spectrum of particles radiating in a uniform field is nowhere harder than an  $\omega^{1/3}$  power law, which, since harder spectra have been observed in gamma-ray bursts, has led to the discussion of a synchrotron ‘line of death’ (Preece et al. 1998). Our results confirm that this is generally true for isotropic particle distributions in large scale, static, 3D turbulence. However, in agreement with other treatments (Fleishman & Urtiev 2010) we find that, in the presence of large amplitude turbulence on short length-scales, the low-frequency asymptote can diverge from this value. We find low frequency spectra that are typically harder than  $\omega^{1/3}$ . For fields with  $a \gg 1$  the spectrum exhibits a gradual hardening with the slope increasing approximately 0.05 per decade in frequency. For fields with strength parameters  $a \gtrsim 1$ , low frequency power-law asymptotes are produced,  $F_\omega \propto \omega^q$ , with  $1/3 \leq q \leq 1/2$ . For fields with  $a < 1$  slightly larger values of  $q$  appear to be possi-

ble, although shocks with such small strength parameters are poor accelerators (Kirk & Reville 2010). Spectra as hard as  $\omega^1$  are known to be produced by weak ( $a \ll 1$ ) turbulence that can be factorized into 2D and 1D components (Fleishman 2006b; Medvedev 2006). However, they do not arise in our results, which are based on a

fully 3D turbulence model.

We thank A. M. Taylor and S. O’Sullivan for helpful discussions. B.R. gratefully acknowledges support from the Alexander von Humboldt foundation.

## REFERENCES

- Achterberg, A., Gallant, Y. A., Kirk, J. G., & Guthmann, A. W. 2001, *MNRAS*, 328, 393
- Akhiezer, A. I., & Shul’ga, N. F. 1987, *Soviet Physics Uspekhi*, 30, 197
- Casse, F., Lemoine, M., & Pelletier, G. 2002, *Phys. Rev. D*, 65, 023002
- Derishev, E. V. 2007, *Ap&SS*, 309, 157
- Fleishman, G. D. 2006a, *MNRAS*, 365, L11
- . 2006b, *ApJ*, 638, 348
- Fleishman, G. D. 2006c, in *Lecture Notes in Physics*, Berlin Springer Verlag, Vol. 687, *Geospace Electromagnetic Waves and Radiation*, ed. J. W. Labelle & R. A. Treumann, 87–+
- Fleishman, G. D., & Urtiev, F. A. 2010, *MNRAS*, 406, 644
- Trier Frederiksen, J., Haugbølle, T., Medvedev, M. V., & Nordlund, Å. 2010, *ArXiv e-prints*
- Giacalone, J., & Jokipii, J. R. 1999, *ApJ*, 520, 204
- Ginzburg, V. L. & Syrovatskii S. I., *ARA&A*, 3, 297
- Hededal, C. 2005, PhD thesis, , Niels Bohr Institute
- Kirk, J. G., & Reville, B. 2010, *ApJ*, 710, L16
- Klein, S. 1999, *Reviews of Modern Physics*, 71, 1501
- Landau, L. D., & Lifshitz, E. M. 1971, *The classical theory of fields*, ed. Landau, L. D. & Lifshitz, E. M.
- Landau, L. D., & Pomeranchuk, I. 1953a, *Dokl. Akad. Nauk Ser. Fiz.*, 92, 735
- . 1953b, *Dokl. Akad. Nauk Ser. Fiz.*, 92, 535
- Martins, J. L., Martins, S. F., Fonseca, R. A., & Silva, L. O. 2009a, in *Society of Photo-Optical Instrumentation Engineers (SPIE) Conference Series*, Vol. 7359, *Society of Photo-Optical Instrumentation Engineers (SPIE) Conference Series*
- Martins, S. F., Fonseca, R. A., Silva, L. O., & Mori, W. B. 2009b, *ApJ*, 695, L189
- Medvedev, M. V. 2000, *ApJ*, 540, 704
- . 2006, *ApJ*, 637, 869
- Medvedev, M. V., Trier Frederiksen, J., Haugbølle, T., & Nordlund, Å. 2010, *ArXiv e-prints*
- Melrose, D. B. 1978, *ApJ*, 225, 557
- Migdal, A. B. 1956, *Physical Review*, 103, 1811
- Preece, R. D., Briggs, M. S., Mallozzi, R. S., Pendleton, G. N., Paciesas, W. S., & Band, D. L. 1998, *ApJ*, 506, L23
- Press, W. H., Flannery, B. P., & Teukolsky, S. A. 1986, *Numerical recipes. The art of scientific computing*, ed. Press, W. H., Flannery, B. P., & Teukolsky, S. A.
- Reville, B., & Kirk, J. G. 2010, *ApJ*, 715, 186
- Schwinger, J. 1949, *Physical Review*, 75, 1912
- Schwinger, J., DeRead, L. L., Milton, K. A., & y Tsai, W. 1998, *Classical Electrodynamics* (Perseus Books, Reading)
- Sironi, L., & Goodman, J. 2007, *ApJ*, 671, 1858
- Sironi, L., & Spitkovsky, A. 2009a, *ApJ*, 698, 1523
- . 2009b, *ApJ*, 707, L92
- Spitkovsky, A. 2005, in *American Institute of Physics Conference Series*, Vol. 801, *Astrophysical Sources of High Energy Particles and Radiation*, ed. T. Bulik, B. Rudak, & G. Madejski, 345–350
- Spitkovsky, A. 2008a, *ApJ*, 673, L39
- . 2008b, *ApJ*, 682, L5
- Toptygin, I. N., & Fleishman, G. D. 1987, *Ap&SS*, 132, 213

## APPENDIX

### SYNCHROTRON EMISSION

We start by making a Taylor expansion of the particle position, the deviations from ballistic motion and the phase. This can be achieved using a purely geometric description of the trajectory.

First, define the tangent, normal and binormal unit-vectors:

$$\begin{aligned} \mathbf{T}(t) &= \frac{\beta(t)}{\beta(t)} \\ \mathbf{N}(t) &= \frac{d\mathbf{T}/dt}{|d\mathbf{T}/dt|} = \frac{d\mathbf{T}/dt}{c\beta(t)\kappa(t)} \\ \mathbf{B}(t) &= \mathbf{T}(t) \wedge \mathbf{N}(t) \end{aligned} \tag{A1}$$

The quantity  $\kappa(t)$  is called the curvature of the trajectory. The Frenet-Serret formulae give the evolution of these vectors along the trajectory:

$$\begin{pmatrix} d\mathbf{T}/dt \\ d\mathbf{N}/dt \\ d\mathbf{B}/dt \end{pmatrix} = \begin{pmatrix} 0 & c\beta\kappa & 0 \\ -c\beta\kappa & 0 & c\beta\bar{\tau} \\ 0 & -c\beta\bar{\tau} & 0 \end{pmatrix} \begin{pmatrix} \mathbf{T} \\ \mathbf{N} \\ \mathbf{B} \end{pmatrix} \tag{A2}$$

where  $\bar{\tau}$  is called the torsion of the trajectory.



Therefore,

$$\begin{aligned} \delta \mathbf{R}(t, \tau) &= \left[ \frac{\tau^2}{2} c \dot{\beta} + \frac{\tau^3}{6} (c \ddot{\beta} - c^3 \beta^3 \kappa^2) \right] \mathbf{T} \\ &\quad + \left[ \frac{\tau^2}{2} c^2 \beta^2 \kappa + \frac{\tau^3}{6} (3c^2 \beta \dot{\beta} \kappa + c^2 \beta^2 \dot{\kappa}) \right] \mathbf{N} + \frac{\tau^3}{6} c^3 \beta^3 \kappa \bar{\tau} \mathbf{B} + \mathcal{O}(\tau^4) \end{aligned} \quad (\text{A3})$$

$$\begin{aligned} \delta \boldsymbol{\beta}(t, \tau) &= \left[ \tau \dot{\beta} + \frac{\tau^2}{2} (\ddot{\beta} - c^2 \beta^3 \kappa^2) \right] \mathbf{T} + \left[ \tau c \beta^2 \kappa + \frac{\tau^2}{2} (3c \beta \dot{\beta} \kappa + c \beta^2 \dot{\kappa}) \right] \mathbf{N} \\ &\quad + \frac{\tau^2}{2} c^2 \beta^3 \kappa \bar{\tau} \mathbf{B} + \mathcal{O}(\tau^3) \end{aligned} \quad (\text{A4})$$

Then, using

$$\boldsymbol{\beta} \cdot \delta \mathbf{R} / c = \frac{\tau^2}{2} \beta \dot{\beta} + \frac{\tau^3}{6} (\beta \ddot{\beta} - c^2 \beta^4 \kappa^2) + \mathcal{O}(\tau^4) \quad (\text{A5})$$

$$(\delta \mathbf{R})^2 / c^2 = \frac{\tau^4}{4} (\dot{\beta}^2 + c^2 \beta^4 \kappa^2) + \mathcal{O}(\tau^5) \quad (\text{A6})$$

one finds

$$\delta \Delta(t, \tau) = \left[ \tau^2 \beta^2 + 2\tau \boldsymbol{\beta} \cdot \delta \mathbf{R} / c + (\delta \mathbf{R})^2 / c^2 \right]^{1/2} - |\tau| \beta \quad (\text{A7})$$

$$= \frac{\tau |\tau|}{2} \dot{\beta} + \frac{|\tau^3|}{24} (4\ddot{\beta} - c^2 \beta^3 \kappa^2) + \mathcal{O}(\tau^4) \quad (\text{A8})$$

Substituting into the definition of the phase-lag:

$$g(t, \tau) = \omega \tau \left[ 1 - \beta - \frac{\tau}{2} \dot{\beta} - \frac{\tau^2}{24} (4\ddot{\beta} - c^2 \beta^3 \kappa^2) \right] + \mathcal{O}(\tau^4) \quad (\text{A9})$$

$$\dot{g} = \omega \left[ 1 - \beta - \tau \dot{\beta} - \frac{\tau^2}{8} (4\ddot{\beta} - c^2 \beta^3 \kappa^2) \right] + \mathcal{O}(\tau^3) \quad (\text{A10})$$

At this point, two additional assumptions are introduced:

1. the electromagnetic fields are constant over a photon formation length, i.e.,  $\ddot{\beta} = 0$
2. *linear acceleration emission* is negligible, i.e.,  $\dot{\beta} = 0$

The first is an implicit condition for the validity of a PIC simulation, when the photon formation time is comparable or shorter than the time step. The second is fulfilled under normal conditions ( $|E| \lesssim |B|$ ).

Then, writing

$$x = \frac{c \kappa \gamma \tau}{2} \quad (\text{A11})$$

$$\omega_c = \frac{3}{2} \gamma^3 c \kappa \quad (\text{A12})$$

one finds

$$\begin{aligned} g(t, \tau) &\approx \omega \tau \left[ 1 - \beta + \frac{1}{24} c^2 \beta^3 \kappa^2 \tau^2 \right] \\ &\approx \frac{3\omega}{2\omega_c} \left[ x + \frac{x^3}{3} \right] \end{aligned} \quad (\text{A13})$$

$$\dot{g} \approx \omega \left[ 1 - \beta - \tau \dot{\beta} - \frac{\tau^2}{8} (4\ddot{\beta} - c^2 \beta^3 \kappa^2) \right] + \mathcal{O}(\tau^3) \quad (\text{A14})$$

and

$$\dot{g}(t, \tau) \approx \frac{3\gamma \omega c \kappa}{4\omega_c} (1 + x^2) \quad (\text{A15})$$

At the frequencies of interest ( $\omega \sim \omega_c$ ), the dominant contribution to the integrals, which arises for  $g \sim 1$ , occurs for  $x \sim 1$ . In this case, the contribution of the first two non-vanishing terms in the Taylor expansions of both  $g$  and  $\dot{g}$  are comparable. Thus, in expanding the integrands in (18) it is necessary to include both these terms, whereas the lowest order non-vanishing contributions to  $\delta \Delta$  and  $\boldsymbol{\beta} \cdot \delta \boldsymbol{\beta}$  are sufficient.

The instantaneous power (18) is then

$$P(\omega, t) \approx \frac{e^2 \omega}{\pi c} \frac{4}{3\gamma^2} \int_0^\infty dx \frac{\left(x^2 + \frac{x^4}{2}\right)}{x + \frac{x^3}{3}} \sin \left[ \frac{3\omega}{2\omega_c} \left(x + \frac{x^3}{3}\right) \right] \quad (\text{A16})$$

Writing  $\eta = \omega/\omega_c$ ,

$$\frac{d}{d\eta} \left( \frac{1}{\eta} P \right) = \frac{e^2}{\pi c} \frac{2\omega_c}{\gamma^2} \int_0^\infty dx \left(x^2 + \frac{x^4}{2}\right) \cos \left[ \frac{3\eta}{2} \left(x + \frac{x^3}{3}\right) \right] \quad (\text{A17})$$

Then, using

$$\frac{1}{\sqrt{3}} K_{2/3}(\eta) = \int_0^\infty dx x \sin \left[ \frac{3\eta}{2} \left(x + \frac{x^3}{3}\right) \right] \quad (\text{A18})$$

to find

$$\mathcal{I}_2 \equiv \int_0^\infty dx x^2 \cos \left[ \frac{3\eta}{2} \left(x + \frac{x^3}{3}\right) \right] = \frac{1}{\sqrt{3}} \left[ K'_{2/3}(\eta) + \frac{2}{3\eta} K_{2/3}(\eta) \right] \quad (\text{A19})$$

$$\mathcal{I}_4 \equiv \int_0^\infty dx x^4 \cos \left[ \frac{3\eta}{2} \left(x + \frac{x^3}{3}\right) \right] = \frac{2}{\sqrt{3}} K'_{2/3}(\eta) - 3\mathcal{I}_2 \quad (\text{A20})$$

and noting that

$$\frac{d}{d\eta} K_{2/3}(\eta) - \frac{2}{3\eta} K_{2/3}(\eta) = -K_{5/3}(\eta) \quad (\text{A21})$$

one arrives at the standard expression for angle-integrated synchrotron radiation

$$P(\eta, t) = \frac{\sqrt{3} e^2 \gamma \kappa}{2\pi} \eta \int_\eta^\infty dx K_{5/3}(x) \quad (\text{A22})$$